PtSn/C electrocatalysts modified with Ni and Ga for the ethanol electrooxidation

Giordano T. Paganoto and Josimar Ribeiro*

Departamento de Química, Centro de Ciências Exatas, Universidade Federal do Espírito Santo, Av. Fernando Ferrari, 514, CEP.: 29075-910, Vitória, Espírito Santo, Brazil

*Corresponding author

DOI: 10.5185/amlett.2018.1875
www.vbripress.com/aml

Abstract

Ni and Ga elements are inexpensive compared to the Pt. Ni and NiO_x have been recognized to have potential applications in ethanol electrooxidation. For these reasons and based on previous results obtained with Ga addition on Pt-based electrocatalysts we have investigated the PtSn/C electrocatalysts modified with Ni and Ga. The PtSnNiGa/C electrocatalysts were characterized in acidic medium by electrochemical techniques and by physicochemical techniques such as: X-ray diffraction; Energy dispersive X-ray spectroscopy; Transmission electron microscopy. Based on the TEM analyses, the PtSnNiGa/C electrocatalysts show average particle sizes range between 3.6 – 5.5 nm, which is consistent with XRD data. The ethanol oxidation on the PtSnNiGa/C electrocatalysts occur at lower potentials as compared to the Pt/C. The higher current normalized by Pt mass (2.62 Ag^{-1}_{Pt}), lower susceptibility to poisoning anodic and charge transfer resistance (245 Ω) were obtained for the $Pt_{45}Sn_{22}Ni_{21}Ga_{12}$/C electrocatalyst. The current normalized by Pt mass: $Pt_{50}Sn_{26}Ni_{12}Ga_{12}$/C (2.8 Ag^{-1}_{Pt}); $Pt_{45}Sn_{22}Ni_{21}Ga_{12}$/C (2.62 Ag^{-1}_{Pt}); $Pt_{52}Sn_{21}Ni_{18}Ga_{9}$/C (1.63 Ag^{-1}_{Pt}) and $Pt_{43}Sn_{23}Ni_{11}Ga_{22}$/C (1.27 Ag^{-1}_{Pt}) electrocatalysts are higher compared to binary catalysts with high Pt content. The promotion effect of PtSnNiGa/C to ethanol electrooxidation can be explained by the modification structural of Pt by incorporation of Sn, Ni and/or Ga to the face-centered cubic crystalline of Pt.

Keywords: Ethanol oxidation reaction, gallium, platinum, fuel cells, quaternary electrocatalysts.

Introduction

Considering the growing debate over the use of fossil fuels and global climate change, fuel cell technology has emerged as a clean and efficient source of energy in the world as compared to combustion engines [1-5].

In the development of PEMFCs (polymer electrolyte membrane fuel cells), ethanol has been shown to be a good alternative to hydrogen as a fuel in the cell, for example, ethanol is less toxic than methanol and has a theoretical energy density of 8.0 kWh kg^{-1} against 6.0 kWh kg^{-1} for methanol [6]. In Brazil, the structure of the biofuels production chain (biodiesel and bioethanol) makes fuel cells with direct ethanol insertion a promising source of energy in the long term [7].

The complete oxidation of the ethanol to form CO_2 and to provide 12e is kinetically unfavorable due to the difficulty of breaking the C-C bond in the ethanol molecule. In this way, acetaldehyde and acetic acid are formed in greater quantity by means of the partial oxidation involving, respectively, 2e or 4e [1-3]. The ethanol oxidation reaction (EOR) occurs through a mechanism that involves reactions of adsorbed intermediates and products of incomplete oxidation of ethanol [8]. The main intermediates identified are carbon monoxide adsorbed on the surface of the catalyst (CO_{ads}) and hydrocarbon residues C1 and C2, whereas the main products are acetaldehyde and acetic acid [1-3, 8]. In the oxidation mechanism of ethanol in Pt catalysts proposed by Lamy et al. [9], the first step consists of the adsorption dissociation of an ethanol molecule at the active site of the metal and the first product to be formed is acetaldehyde, which requires transfer of only 2e, which can be oxidized to acetic acid or carbon monoxide with methane generation at low potential (<0.2 V vs RHE, reversible hydrogen electrode) [8, 9]. The oxidation of acetic acid at low temperatures is kinetically unfavorable, therefore, acid formation can be considered the final step of the mechanism.

An efficient catalyst should facilitate the dehydrogenation of the ethanol molecule, the breakdown of the C-C bond and the oxidation of the CO_{ads} species. In addition, the activation of the water molecule at low potential is crucial for the oxidation of the CO_{ads} and the adsorbed intermediates at the active sites of the catalyst [10, 11]. PtSn/C and PtRu/C electrocatalysts are the most efficient for ethanol oxidation reaction [8]. The addition of Sn increases the distance of the Pt-Pt bond, which facilitates the dissociative adsorption of ethanol to smaller potentials [12]. The insertion of Ni and Ti into PtSn/C electrocatalysts promotes the increase in electrocatalytic activity, since the synergistic effect of Ni

and Ti is related to the activation of water molecules in smaller potentials [13]. The use of Ti and Ni elements favors the formation of acetaldehyde as the main product of the ethanol oxidation reaction [13].

Gallium is widely used mainly in the forms of GaAs, GaN and GaP to manufacture integrated circuits for cell phones, solar cells and light emitting diodes (LEDs) [14]. Few information has been found in the literature on the use of Ga as electrocatalysts for alcohol oxidation. Hogarth *et al.* [15] showed that the PtGa/C binary catalyst supported on Vulcan XC72R carbon promotes the oxidation of methanol at lower potentials than the Pt/C, PtPd/C and PtOs/C catalysts. The study conducted by Kumar *et al.* [16] showed that Pt (IV) can react with fused Ga through the sonication of a mixture of a solution of H_2PtCl_6 with the Ga liquid to form the $GaPt_2$ and $GaPt_3$ metal alloys. The presence of Ga shifts the center of the d-band of Pt to values smaller than the Fermi level of pure Pt, weakening the interaction between Pt and CO_{ads} [16].

The oxides of Ga, α-Ga_2O_3 and β-Ga_2O_3, are also capable of promoting the oxidation of methanol. According to the mechanism investigated by Collins *et al.* [17] by means of the programmed temperature reaction surface analysis using Fourier transform infrared spectroscopy, methanol can adsorb on the surface of the GaO oxides, forming the methoxy, methyl group, carbon monoxide and hydroxyl group. Recently, one has been reported that a small Ga addition to Pt/C electrocatalyst reduce onset potential towards ethanol electrooxidation [18, 19]. Thus, this paper reports a systematic physicochemical and electrochemical investigation of PtSnNiGa/C electrocatalysts toward ethanol oxidation reaction.

Experimental

Material synthesis

PtSnNiGa/C electrocatalysts were synthesized by the thermal decomposition of polymeric precursors method (DPP); the procedure described elsewhere [13, 18, 19] as followed. Briefly, for example, the Pt-resin (material precursor $H_2PtCl_6.H_2O$ - Sigma-Aldrich) was mixed with citric acid (Neon) and ethylene glycol (Sigma-Aldrich) in a beaker in a water bath at 60-65°C; a 1:4:16 Pt/citric acid/ethylene glycol molar ratio was employed. Afterwards, the temperature was raised to 80-85°C, the mixture was kept stirring for 1h. All the metal-resin using in this investigation were prepared in this way. The synthesis of PtSnNiGa/C was made using amounts appropriated each metal-resin. For more details please check the reference [19].

Physical characterizations

The X-ray diffraction (XRD) patterns were obtained on a Bruker D8 diffractometer operating with Cu Kα radiation (λ = 1.5406 Å), with a scan in 2θ from 10° to 90° and step rate of 0.01° min^{-1}. The crystallite size (D) was estimated by using the Scherrer's ($D = (0.9 \times \lambda)/(B \times \cos\theta)$ eq. (1)) [20] and the cell parameters (a_{cell} and V_{cell}) were calculated by a computer program which considered the unit cell parameters using the least-squares method.

The morphology and the particle size distribution of the PtSnNiGa/C electrocatalysts were evaluated by Transmission Electron Microscopy (TEM), conducted on a JEOL /JEM-1400 model microscope. The experimental composition of the PtSnNiGa/C electrocatalysts was obtained using a scanning electron microscope Carl Zeiss EVO 10 model coupled with energy-dispersive X-ray spectroscopy (SEM-EDS).

Electrochemical measurements

The electrochemical profile of the PtSnNiGa/C electrocatalysts was obtained by cyclic voltammetry (CV) in N_2-purged 0.5 mol L^{-1} H_2SO_4 (Sigma-Aldrich) solution. Measurements were conducted in an electrochemical cell that included a graphite electrode with a geometric area of 4 cm^2 as counter electrode and a $Ag/AgCl_{KClsat}$ electrode as the reference electrode. The working electrode was prepared by depositing 100 µL of electrocatalyst ink, which was consisting of 1 mg of electrocatalyst and 100 µL of a mixture of (5 µL) Nafion® and (95 µL) ethanol (Sigma-Aldrich) on a graphite electrode previously polished (0.16 cm^2 geometric area). Activity and stability analysis were carried out by cyclic voltammetry, chronopotentiometry, and chronoamperometry in the presence of 1.0 mol L^{-1} ethanol and 0.5 mol L^{-1} H_2SO_4. The electrochemical impedance spectroscopy (EIS) was carried out in presence and absence of 1.0 mol L^{-1} at 0.2 V vs $Ag/AgCl_{KClsat}$.

Results and discussion

EDS results show that the PtSnNiGa/C electrocatalyst experimental compositions are close to the nominal compositions (see Figure S1 in the supplementary material). However, the $Pt_{50}Sn_{26}Ni_{12}Ga_{12}/C$ (nominal composition = $Pt_{50}Sn_{20}Ni_{15}Ga_{15}/C$) and $Pt_{43}Sn_{23}Ni_{11}Ga_{22}/C$ electrocatalysts (nominal composition = $Pt_{50}Sn_{20}Ni_{10}Ga_{20}/C$) showed a slight amount of Sn higher than the nominal compositions. Moreover, the last one electrocatalyst and the $Pt_{45}Sn_{22}Ni_{21}Ga_{12}/C$ (nominal composition = $Pt_{50}Sn_{20}Ni_{25}Ga_5/C$ showed a slight decrease in the amount of Pt **(see Table 1).** Nevertheless, the results obtained by the EDS analyses showed that DDP process is an adequate method to prepared this kind of material.

Fig. 1 shows the X-ray diffraction pattern of the PtSnNiGa/C electrocatalysts supported on Vulcan XC72 carbon. The diffraction angles shown in **Fig. 1** are shifted to smaller values than the 2θ angles pure Pt cubic structure probably due to the incorporation of Sn (atomic radius = 151pm) to the Pt cubic structure, increasing the value of the lattice parameter, a_{cell}, (from 3.9280 Å to 3.9436 Å), since the values of a are larger when

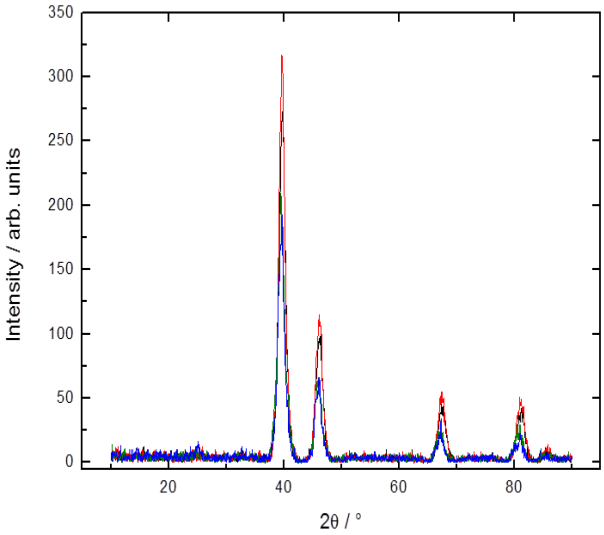

Fig. 1. XRD patterns of the PtSnNiGa/C electrocatalysts: (black line) $Pt_{45}Sn_{22}Ni_{21}Ga_{12}/C$ (red line) $Pt_{52}Sn_{21}Ni_{18}Ga_9/C$ (green line) $Pt_{50}Sn_{26}Ni_{12}Ga_{12}/C$ (blue line) $Pt_{43}Sn_{23}Ni_{11}Ga_{22}/C$.

compared to the pure Pt (a = 3.923 Å) [21]. Although the main hypothesis is that the Sn atoms are incorporated into the crystalline structure of Pt and may form some type of solid substitutional solution, it is possible that Ga and Ni are also incorporated into the Pt structure in smaller amounts. The formation of an interstitial solid solution should be discarded because the atomic radius of Sn (151 pm), Ni (125 pm) and Ga (122 pm) are larger than octahedral interstices (57 pm) and tetrahedral (31 pm). In addition, it is noted that it is not possible to observe a separation phases by means of the formation of Ni and/or Ga crystalline structure, even in electrocatalysts with the higher amounts of these metals. Nevertheless, it is possible observe that the Pt/Sn and Ni/Ga ratio show a pattern as a function of the a_{cell}. For example, $Pt_{44.6}/Sn_{22.4}$ = 1.99; $Pt_{51.7}/Sn_{20.8}$ = 2.49; $Pt_{50.0}/Sn_{25.9}$ = 1.93 and $Pt_{43.0}/Sn_{23.2}$ = 1.85 ranging from 1.85 to 2.49. And the Ni/Ga ratio: $Ni_{20.9}/Ga_{12.1}$ = 1.73; $Ni_{18.6}/Ga_{8.9}$ = 2.09; $Ni_{12.5}/Ga_{11.6}$ = 1.08 and $Ni_{11.3}/Ga_{22.5}$ = 0.50 ranging from 0.50 to 2.09. These results suggesting the possible incorporation of Ni to the PtSn structure leading to decrease of a_{cell}, that is, the Ni-richer the electrocatalyst lower the a_{cell}. Analyzing the crystallite sizes of **Table 1**, there is no direct relationship between the composition of the quaternary catalysts and the crystallite size. In addition, it is noted that crystallites have apparently radial growths, since the growth is almost uniform in all planes (6.5 nm – 8.2 nm).

The mean particle sizes obtained from the TEM images **(see Fig. 2)** show that the $Pt_{50}Sn_{26}Ni_{12}Ga_{12}/C$ and $Pt_{43}Sn_{23}Ni_{11}Ga_{22}/C$ electrocatalysts have slightly smaller particle sizes than the crystallite sizes estimated by XRD data, this may be related to the fact that the particles of these electrocatalysts are not well-defined spherical [22]. Even so, all electrocatalysts have particle sizes like those found in the literature (2 nm to 7 nm) [4, 6, 13, 18, 19].

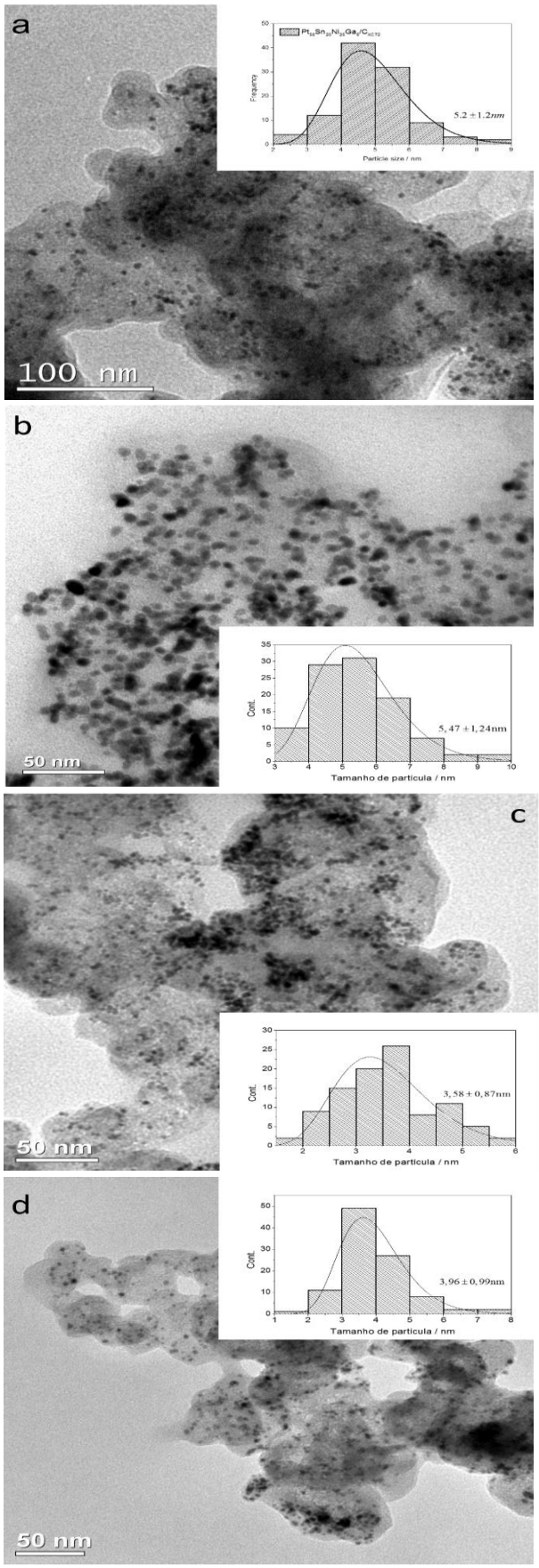

Fig. 2. TEM images and histograms of the electrocatalysts: (a) $Pt_{45}Sn_{22}Ni_{21}Ga_{12}/C$ (b) $Pt_{52}Sn_{21}Ni_{18}Ga_9/C$ (c) $Pt_{50}Sn_{26}Ni_{12}Ga_{12}/C$ (d) $Pt_{43}Sn_{23}Ni_{11}Ga_{22}/C$.

Table 1. EDS and XRD results obtained for the PtSnNiGa/C electrocatalysts.

Electrocatalysts							
Nominal composition	**Experimental composition**	a_{cell} / Å	V_{cell} / Å^3	***D*** **/nm**			
				111	**200**	**220**	**311**
$Pt_{50}Sn_{20}Ni_{25}Ga_5/C$	$Pt_{45}Sn_{22}Ni_{21}Ga_{12}/C$	3.9280	60.62±0.07	7.1	7.0	7.2	7.6
$Pt_{50}Sn_{20}Ni_{20}Ga_{10}/C$	$Pt_{52}Sn_{21}Ni_{18}Ga_9/C$	3.9298	60.69±0.07	7.7	7.5	7.7	8.1
$Pt_{50}Sn_{20}Ni_{15}Ga_{15}/C$	$Pt_{50}Sn_{26}Ni_{12}Ga_{12}/C$	3.9433	61.32±0.04	6.5	7.5	7.8	7.6
$Pt_{50}Sn_{20}Ni_{10}Ga_{20}/C$	$Pt_{43}Sn_{23}Ni_{11}Ga_{22}/C$	3.9436	61.33±0.06	7.3	7.9	8.2	7.2

Fig. 3 depicts the cyclic voltammograms in the cycles 50, 500 and 1000 of the PtSnNiGa/C electrocatalysts in supporting electrolyte, recorded at range from -0.2 to 1.0 V vs. $Ag/AgCl_{KClsat}$. All the electrocatalysts exhibited a very similar profile in the 50 cycles, which are close to the behavior already presented by Pt-based electrocatalysts supported on Vulcan carbon [4, 6, 13, 18, 19]. Poorly defined hydrogen adsorption / desorption region (-0.2 and 0.1 V vs. $Ag/AgCl_{KClsat}$) as compared to the well-defined H_2 peaks for pure Pt is due to the formation of Sn and Ni oxide/hydroxide layers that can block the active sites of Pt [13, 19].

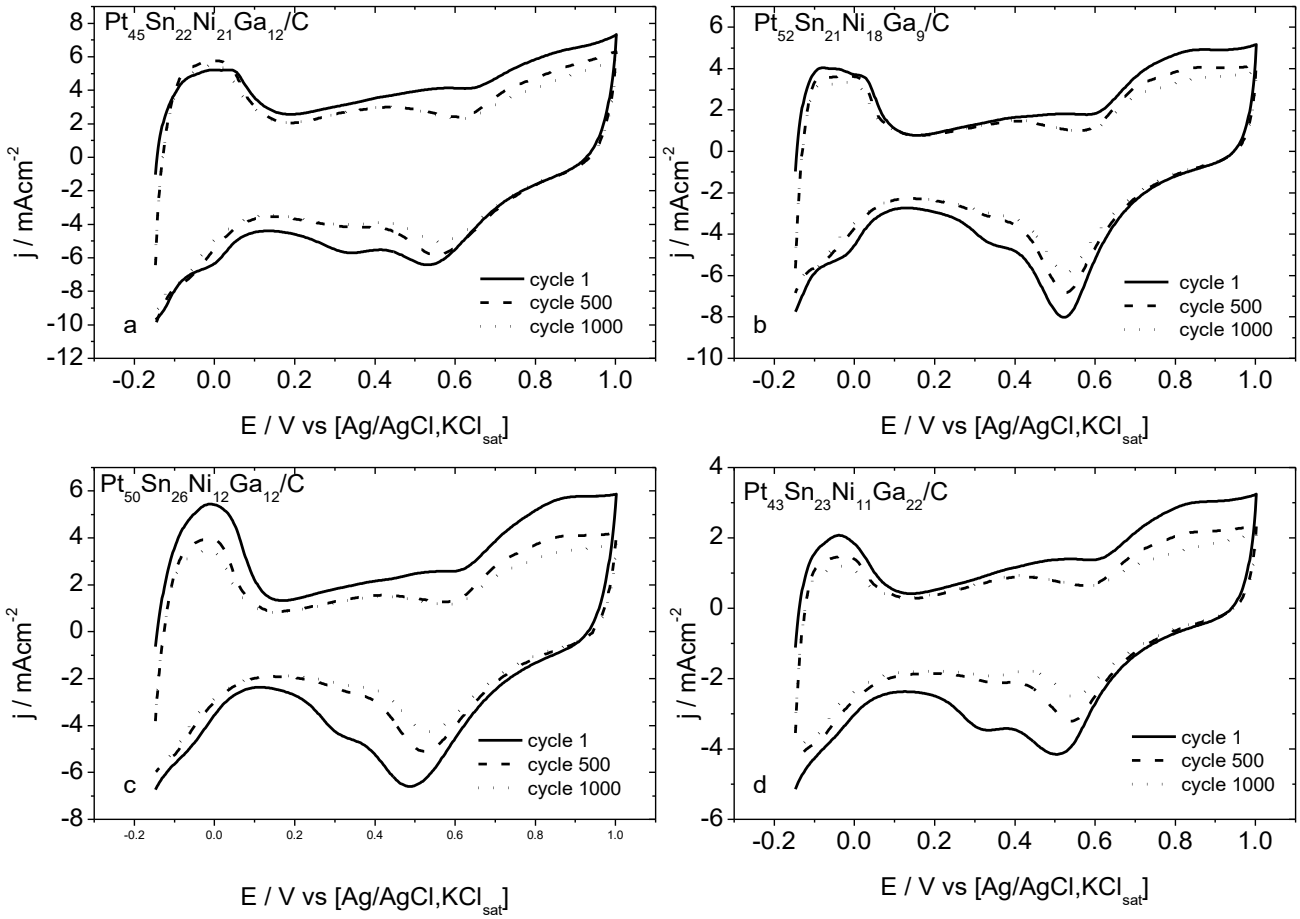

Fig. 3. Cyclic voltammograms of the PtSnNiGa/C electrocatalysts in 0.5 mol L^{-1} H_2SO_4 supporting electrolyte at 20 mV s^{-1}. (a) $Pt_{45}Sn_{22}Ni_{21}Ga_{12}/C$; (b) $Pt_{52}Sn_{21}Ni_{18}Ga_9/C$; (c) $Pt_{50}Sn_{26}Ni_{12}Ga_{12}/C$ and (d) $Pt_{43}Sn_{23}Ni_{11}Ga_{22}/C$.

All the electrocatalysts present oxidation peak between 0.7 V and 0.9 V vs. $Ag/AgCl_{KClsat}$. This oxidation peak could be associated to carbon support or Ni/Ga oxides present in the electrocatalysts [19, 23]. After 1000 CV cycles the charge densities, for all the electrocatalysts, decrease maybe due to the metal dissolution. To evaluate the stability of the PtSnNiGa/C electrocatalysts, we estimated the EASA (Electrochemical Active Surface Area) by EASA = $q_H/(0.21\times[Pt])$ equation, the procedure was described elsewhere [19]. With exception of the $Pt_{45}Sn_{22}Ni_{21}Ga_{12}/C$ electrocatalyst, all the electrocatalysts present a large decrease in the EASA values after 1000 CV cycles (see Table S1 in the supplementary material).

The **Fig. 4** shows the voltammetric curves of the PtSnNiGa/C electrocatalysts recorded in the presence of ethanol 1.0 molL^{-1}. In the lower potential range (-0.2 to 0.0 V vs. Ag/AgCl$_{KClsat}$), the adsorption of ethanol molecules on the electrode surface suppressed the hydrogen adsorption/desorption peaks, it was already observed before for other Pt-based electrocatalysts [13, 18, 19]. For better viewing, the **Fig. 4A** was divided in positive going potential scan **(Fig. 4B)** and negative going potential scan **(Fig. 4C)**. Thus, at low potentials, peaks (1) and (2) can be attributed to the formation of acetaldehyde and activation of the water molecules. At high potentials, peak (3) is related to the formation of acetic acid. In the negative going potential scan, all the PtSnNiGa/C electrocatalysts have the peak (4) which may be related to oxidation of species such as CH_x and CO_{ads} and peak (5) may represent the oxidation of ethanol on the reactivated surface of Pt [24]. Table S2, in the supplementary material, show the potentials and currents normalized by the Pt loading at the peaks (1) - (5). Note that $Pt_{50}Sn_{26}Ni_{12}Ga_{12}/C$ does not show peaks (1) and (2), and the peak (3) occurs at slightly higher potentials for $Pt_{50}Sn_{26}Ni_{12}Ga_{12}/C$ and $Pt_{43}Sn_{23}Ni_{11}Ga_{22}/C$ compared to the other electrocatalysts investigated in this paper. This result indicates that probably the formation of acetic acid occurs at higher potentials for these materials.

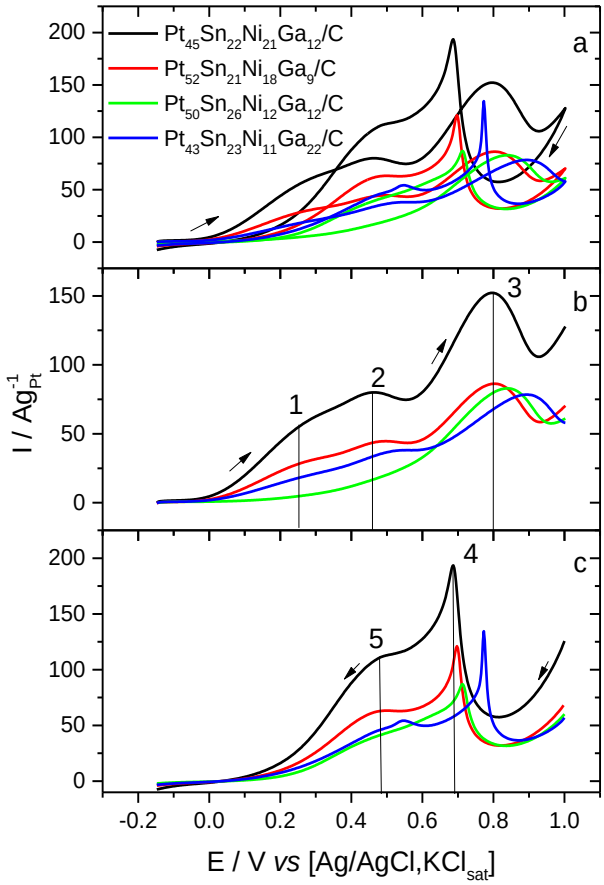

Fig. 4. (a) Cyclic voltammograms of the PtSnNiGa/C electrocatalysts in presence of ethanol 1.0 mol L^{-1} + 0.5 mol L^{-1} H_2SO_4 supporting electrolyte at 20 mV s^{-1}; (b) positive-going potential scan and (c) negative-going potential scan.

Chronoamperograms of the quaternary $Pt_{45}Sn_{22}Ni_{21}Ga_{12}/C$, $Pt_{52}Sn_{21}Ni_{18}Ga_9/C$, $Pt_{50}Sn_{26}Ni_{12}Ga_{12}/C$ and $Pt_{43}Sn_{23}Ni_{11}Ga_{22}/C$ electrocatalysts are shown in the **Fig. 5A**. The Sn-rich electrocatalyst ($Pt_{50}Sn_{26}Ni_{12}Ga_{12}/C$) showed the higher current value normalized by Pt-loading (2.8 Ag^{-1}$_{Pt}$). However, the Ga-rich electrocatalyst ($Pt_{43}Sn_{23}Ni_{11}Ga_{22}/C$) presented the lower I-value (1.27 Ag^{-1}$_{Pt}$). Compared with other electrocatalysts reported in the literature [13, 19, 25, 26] (see Table S3 in the supplementary material), it is possible to observe that the quaternary electrocatalysts prepared in this investigation present higher current values than other Pt-based electrocatalysts with large Pt loading. For example, comparing the $Pt_{90}Sn_{10}/C$ and $Pt_{50}Sn_{26}Ni_{12}Ga_{12}/C$ electrocatalysts, the reduction of 40 % Pt loading in this material did not lead to loss of activity. One can infer that the synergic effect of Pt, Sn, Ni and Ga elements present in this material promote the ability to oxidize the ethanol. In these electrocatalysts, it is possible to observe that the Pt/Sn ratio is 9 and 1.9, and the a_{cell} is 3.907 Å [25] and 3.943 Å, respectively. These results indicate that the Sn modify the crystalline structure of Pt, which can to influence the ethanol oxidation. Moreover, the presence of Ni/Ga ratio = 1.08 has important role in the ethanol oxidation reaction because the electrocatalytic activity of the quaternary electrocatalyst did not reduced.

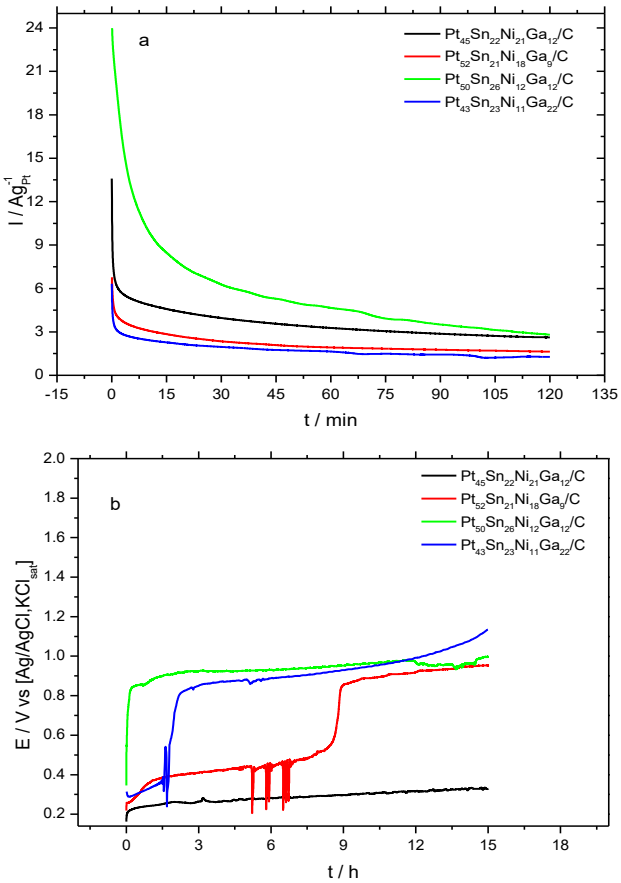

Fig. 5. (a) CA at 0.2 V vs. Ag/AgCl$_{KClsat}$ and (b) CP at 3.0 mA cm^{-2} of the PtSnNiGa/C electrocatalysts in presence of ethanol 1.0 mol L^{-1} + 0.5 mol L^{-1} H_2SO_4 supporting electrolyte.

Chronopotentiograms of the quaternary $Pt_{45}Sn_{22}Ni_{21}Ga_{12}/C$, $Pt_{52}Sn_{21}Ni_{18}Ga_9/C$, $Pt_{50}Sn_{26}Ni_{12}Ga_{12}/C$ and $Pt_{43}Sn_{23}Ni_{11}Ga_{22}/C$ electrocatalysts with the application of a current density 3 mA cm^{-2} for 15 h are shown in the **Fig. 5B.** It is noted that the PtSnNiGa/C electrocatalysts have different behaviors for the ethanol oxidation, for example, the $Pt_{45}Sn_{22}Ni_{21}Ga_{12}/C$ presents the increasing potential over time and does not present the oscillatory behavior characteristic of CO_{ads} poisoning, the main product of the electrochemical reaction, is probably acetaldehyde once the potential reached is less than 0.4 V; $Pt_{50}Sn_{26}Ni_{12}Ga_{12}/C$ shows the increasing potential over time, indicating that the ethanol oxidation occurs with low electrode poisoning, as the potential reached after the first few hours of experiment is approximately 0.9 V, it is possible that there is the formation of acetic acid; $Pt_{52}Sn_{21}Ni_{18}Ga_9/C$ shows the profile with increasing potential up to approximately 5h, after this period the oscillatory behavior occurs, indicating the occurrence of the formation of a CO film, after the period of 9h, the potential increases again and remains practically constant in approximately 0.9 V until the end of the experiment.

A similar behavior occurs with $Pt_{43}Sn_{23}Ni_{11}Ga_{22}/C$, so that, the oscillatory behavior occurs around 1.5h, and from 3h of experiment, the electrocatalyst exhibits increasing potential over time. $Pt_{50}Sn_{26}Ni_{12}Ga_{12}/C$ until reaching approximately 0.8 V favoring the formation of the most oxidized species. Although acetaldehyde is the main product formed at low potentials (< 0.4 V vs $Ag/AgCl_{KClsat}$) the formation of CO_2 cannot be ruled out since this process can also occur at low potentials (< 0.3 V vs $[Ag/AgCl_{KClsat}]$) [9]. According to the Wang et al. [8] about 5% of the amount of ethanol is oxidized to CO_2.

Fig. 6 depicts the Nyquist and Bode plots for the quaternary PtSnNiGa/C electrocatalysts in presence of 1.0 mol L^{-1} solution at 0.2 V vs. $Ag/AgCl_{KClsat}$. It is possible observe that the EIS profile is the same for all the electrocatalysts investigated in this paper. The long arcs **(Fig. 6A)** indicate a slow rate for ethanol oxidation reaction (EOR). Parameter values obtained by simulated [R1(R2[CPE1W])] circuit for the PtSnNiGa/C electrocatalysts are shown in the **Table 2**. The charge transfer resistance, R2, shows a great dependence on the composition of electrocatalyst. It ranges from 471 Ω to 2779 Ω in absence of ethanol and from 168 Ω to 814 Ω in presence of ethanol. This suggests that a R2 is related to the EOR. The lower R2-value was obtained for the $Pt_{50}Sn_{26}Ni_{12}Ga_{12}/C$, this result corroborates with the CV and Chrono-data, which showed that this material has the best electrocatalytic activity for ethanol oxidation. Bode plot **(Fig. 6B)** also shows that $Pt_{50}Sn_{26}Ni_{12}Ga_{12}/C$ electrocatalyst exhibit the largest phase angle deviation (~70°), this indicates a larger pore size distribution.

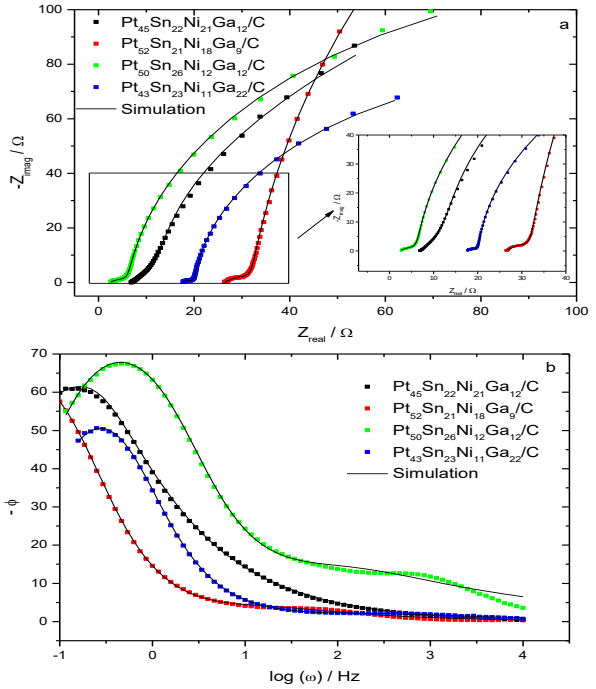

Fig. 6. (a) Nyquist and (b) Bode plots of the different PtSnNiGa/C electrocatalysts supported on Vulcan XC72 carbon prepared by DPP process.

Table 2. Parameter values obtained by simulated [R1(R2[CPE1W])] circuit for the PtSnNiGa/C electrocatalysts in presence and absence of ethanol 1.0 mol L^{-1} + 0.5 mol L^{-1} H_2SO_4 supporting electrolyte.

	$Pt_{45}Sn_{22}Ni_{21}Ga_{12}/C$	$Pt_{52}Sn_{21}Ni_{18}Ga_9/C$	$Pt_{50}Sn_{26}Ni_{12}Ga_{12}/C$	$Pt_{43}Sn_{23}Ni_{11}Ga_{22}/C$
In presence of 1.0 mol L^{-1} of ethanol				
***R*1 / Ω**	6.7	26.04	17.04	2.0
***R*2 / Ω**	245.3	814.0	168	242
***CPE*1 / mF**	10.35	12.04	6.66	5.88
n	0.94	0.95	0.96	0.66
W / Ω	5.2	6.07	4.6	23.64
In 0.5 mol L^{-1} H_2SO_4 supporting electrolyte				
R1 / Ω	6.4	16.08	10.54	41.59
R2 / Ω	471.0	2338	2170	2779
CPE1 / mF	33.0	16.8	7.15	10.7
n	0.97	0.96	0.95	0.95
W / Ω	5.08	2.56	2.58	2.18

χ^2 observed for all simulations ranged from 10^{-4} to 10^{-5} and error for the data-values simulated was obtained between 0.2 – 13%. R1 = ohmic resistance; R2 charge transfer resistance; CPE1 and n = constant phase element and W = Warburg impedance.

Conclusion

The electrocatalytic activity of PtSn/C electrocatalysts supported on Vulcan XC72 carbon, modified with Ni and Ga towards ethanol oxidation was evaluated. The XRD results suggest that the Sn atoms are incorporated into the crystalline structure of Pt and may form some type of solid substitutional solution, it is possible that Ga and Ni are also incorporated into the Pt structure in smaller amounts. The TEM data show that the average particle size of the catalysts is between (3.6 nm and 5.5 nm), which is also compatible with the values reported in the literature. The electrochemical measurements showed that the quaternary electrocatalysts synthesized in this paper present higher normalized current by Pt mass in relation to pure Pt and to other electrocatalysts with high amount of Pt, so that the synthesis of quaternary electrocatalysts with other metals such as Ni and Ga is a viable alternative for the reduction of the Pt loading in electrocatalysts for the ethanol electrooxidation.

Acknowledgements

This work was supported by FAPES, CNPq and CAPES.

Author's contributions

Authors have no competing financial interests.

Supporting information

Supporting informations are available from VBRI Press.

References

1. Wang, Y.; Chen, K. S.; Mishler, J.; Cho, S. C.; Adroher, X. C. *Appl. Energy*, **2011**, *88*, 981. **DOI:** 10.1016/j.apenergy.2010.09.030
2. Rezaei Niya, S. M.; Hoorfar, M. *J. Power Sources*, **2013**, *240*, 281. **DOI:** 10.1016/j.jpowsour.2013.04.011
3. Brouzgou, A.; Song, S. Q.; Tsiakaras, P. *Appl. Catal. B Environ.* **2012**, *127*, 371. **DOI:** 10.1016/j.apcatb.2012.08.031
4. Debe, M. K. *Nature*, **2012**, *486*, 43. **DOI:** 10.1038/nature11115
5. Sharaf, O. Z.; Orhan, M. F. *Renew. Sustain. Energy Rev.* **2014**, *32*, 810. **DOI:** 10.1016/j.rser.2014.01.012
6. Vigier, F.; Coutanceau, C.; Perrard, A.; Belgsir, E. M.; Lamy, C. *J. Appl. Electrochem.* **2004**, *34*, 439. **DOI:** 10.1023/B:JACH.0000016629.98535.ad
7. Moreira, J. R.; Pacca, S. A.; Parente, V. *Energy Policy*, **2014**, *65*, 7. **DOI:** 10.1016/j.enpol.2013.09.055
8. Wang, Y.; Zou, S.; Cai, W.-B. *Catalysts* **2015**, *5*, 1507. **DOI:** 10.3390/catal5031507
9. Vigier, F.; Rousseau, S.; Coutanceau, C.; Leger, J. M.; Lamy, C. *Top. Catal.* **2006**, *40*, 111. **DOI:** 10.1007/s11244-006-0113-7
10. Shao, M. H.; Adzic, R. R. *Electrochim. Acta*, ***2005***, *50*, 2415. **DOI:** 10.1016/j.electacta.2004.10.063
11. Tripkovic, V. *Electrochim. Acta*, **2015**, *168*, 370. **DOI:** 10.1016/j.electacta.2015.04.006
12. Li, H.; Sun, G.; Cao, L.; Jiang, L.; Xin, Q. *Electrochim. Acta*, **2007**, *52*, 6622. **DOI:** 10.1016/j.electacta.2007.04.056
13. Carrareto Caliman, C.; Palma, L. M.; Ribeiro, J. *J. Electrochem. Soc.*, **2013**, *160*, F853. **DOI:** 10.1149/2.073308jes
14. Naumov, A. V.; Naumova, M. A. *Russ. J. non-Ferrous Met.*, **2010**, *51*, 324. **DOI:** 10.3103/S1067821210040127
15. M. P. Hogarth; T. R. Ralph. *Platin. Met. Rev.*, ***2002***, *46*, 146. **DOI:** https://technology.matthey.com/article/46/4/146-164/
16. Kumar, V. B. *et al. Electrochim. Acta*, **2015**, *190*, 659. **DOI:** 10.1016/j.electacta.2015.12.193
17. Collins, S. E.; Baltanás, M. A.; Bonivardi, A. L. *Appl. Catal. A Gen.*, **2005**, *295*, 126. **DOI:** 10.1016/j.apcata.2005.07.053
18. Paganoto, G. T.; Santos, D. M.; Evangelista, T. C. S.; Guimarães, M. C. C.; Carneiro, M. T. W. D; Ribeiro, J. *The Scientific World Journal*, **2017**, *2017*, 1. **DOI:** 10.1155/2017/8786013
19. Santos, D. M.; Paganoto, G. T.; Queiroz, M. A. R.; Guimarães, M. C. C.; Ribeiro, J. *Orbital: The Electronic Journal of Chemistry*, **2017**, *9*, 140. **DOI:** 10.17807/orbital.v9i3.949
20. Cullity, D.; Stock, S. R. Elements of X Ray Diffraction. Prentice Hall Inc.: USA, **2001**.
21. Powder Diffraction File:01-087-0646 Joint Committee on Powder Diffraction Standards Inter. Center for Diffraction Data, v. PDF-2, 2011.
22. Akbari, B.; Tavandashti, M. P.; Zandrahimi, M. *Iran. J. Mater. Sci. Eng.*, **2011**, *8*, 48. **DOI:** http://ijmse.iust.ac.ir/article-1-341-en.html
23. Spinacé, E. V.; Linardi, M.; Neto, A. O. *Electrochem. Commun.*, **2005**, *7*, 365. **DOI:** 10.1016/j.elecom.2005.02.006
24. Sharma, S.; Pollet, B. G. *J. Power Sources*, **2012**, *208*, 96. **DOI:** 10.1016/j.jpowsour.2012.02.011
25. Ribeiro, J. *et al. Electrochim. Acta*, **2007**, *52*, 6997. **DOI:** 10.1016/j.electacta.2007.05.017
26. Almeida, T. S.; Kokoh, K. B.; De Andrade, A. R. *Int. J. Hydrogen Energy*, **2011**, *36*, 3803. **DOI**: 10.1016/j.ijhydene.2010.12.066

